Experimental studies of 3-body correlations in ^{6}He in the quasi-free knockout reaction ^{4}He(^{6}He,2α)2n

S.I. Sidorchuk, A.S. Fomichev, M.S. Golovkov, V.L. Grigorenko, V.A. Gorshkov, A.V. Gorshkov, S.A. Krupko, Yu.Ts. Oganessian, A.M. Rodin, R.S. Slepnev, et al.

Experimental Study of 3-body correlations in ^{6}He in the Quasi-Free Knockout Reaction ^{4}He(^{6}He,2α)2n

S.I. Sidorchuk[1], A.S. Fomichev[1], M.S. Golovkov[1], V.L. Grigorenko[1], V.A. Gorshkov[1], A.V. Gorshkov[1], S.A. Krupko[1], Yu.Ts. Oganessian[1], A.M. Rodin[1], R.S. Slepnev[1], S.V. Stepantsov[1], G.M. Ter-Akopian[1], R. Wolski[2], A.A. Korsheninnikov[3], E.Yu. Nikolskii[3], P. Roussel-Chomaz[4], W. Mittig[4], E.A. Kuzmin[5], B.G. Novatski[5], D.N. Stepanov[5]

[1]Flerov Laboratory of Nuclear Reactions, JINR, 141980 Dubna, Russia
[2]The Henryk Niewodniczanski Institute of Nuclear Physics, Krakow, Poland
[3]RIKEN, Hirosawa 2-1, Wako, Saitama 351-0198, Japan
[4]GANIL, BP 5027, F-14076 Caen Cedex 5, France
[5] The Kurchatov Institute, Kurchatov sq. 1, 123182 Moscow, Russia

Introduction

Quasi-free scattering (QFS) of nucleon and clusters bound in nuclei is acknowledged as a powerful tool for the nuclear structure study [1-3]. Momentum distributions for the knocked-out nucleons and clusters have been extracted from the data of experiments where the remaining third body (spectator) was either nuclear stable or was found in a quasi-stationary state. In many papers the experimental data were analyzed using the Plane Wave Impulse Approximations (PWIA). It was shown by these studies that better correspondence between experimental data and theory predictions can be achieved at higher collision energies. The extension of the PWIA is the Distorted Wave Impulse Approximation (DWIA), in which one takes into account the distortions of the incoming and outgoing waves by using suitable optical model potentials [4]. Even at relatively low beam energy, the use of DWIA allowed the authors to come to more reasonable values of spectroscopic factors and make consistent theoretical predictions for the measured momentum distributions. Results obtained for the QFS reaction ^{6}Li(α,2α)d, studied at the ^{4}He beam energy close to 100 MeV, showed that both the PWIA and DWIA calculations provide rather close descriptions of the experimental data obtained for the ^{6}Li nucleus [5]. Apparently, this could be the case due to the small separation energy known for α cluster in ^{6}Li. This allows one to assume that perhaps QFS data analyzed within the framework of PWIA can be informative for the study of the cluster structures of halo nuclei near the drip-line. In particular one could expect that the reaction of QFS can be used for the direct observation of three-body correlations specific for the ground state of Borromean nuclei.

Helium-6 nucleus is a convenient object to check this assumption as one can believe that the three-body wave function (WF) is well established in theory for this nucleus [6]. However, the peculiarity of ^{6}He consists in the lack of a bound state for the two neutrons becoming free at the knock out of α core. Similar situation occurred when the QFS reactions ^{6}Li(α,2α)pn and ^{6}Li(p,pα)pn were investigated [7,8] for gaining knowledge about the three-body state of ^{6}Li. These experiments were performed in coplanar geometry with the use of so called “point” detectors.

In our experiment we studied the reaction ^{4}He(^{6}He,2α)2n at a ^{6}He beam energy of 25A MeV with emphasis made on the observation of the QFS of ^{4}He target nuclei on α cores bound in the ^{6}He projectile nuclei. We detected two scattered α-particles in a kinematical range corresponding to the QFS whereas two unobserved neutrons were expected to be spectators. For the first time the reaction of QFS was studied in such wide angular range of outgoing α-particles.

Experimental details

The experiment was performed in Dubna at the fragment separator ACCULINNA [9]. The secondary beam of ^{6}He nuclei of the intensity of about $2\cdot10^{4}$ s^{-1} bombarded helium target cooled down to a temperature of about 16 K. The thickness of the target made $2\cdot10^{20}$ cm^{-2}. Standard time-of-flight technique was applied for identification of incoming particles and

measuring their energy. Two multiwire proportional chambers were used for tracking individual beam ions. Two α particles outgoing from the target in angular ranges of ±(15°-55°) were detected in coincidence by means of two identical ΔE-E telescopes. The telescopes installed symmetrically in respect to the beam direction provided for the measurement of X&Y coordinates and the energy of the reaction products. Each telescope consisted of two Si strip detectors (70 μ, 50x50 mm^2 and 1000μ, 61x61 mm^2), used for the measurement of energy loss ΔE, and a 6.2 mm thick Si(Li) detector (66x66 mm^2). The measured energies and angles of the two coincident α-particles allowed calculating the value of the relative momentum of two unobserved neutrons and the momentum vector of their center-of-mass. The background was measured in the run done with the empty target.

Data analysis

For the reaction ^{4}He(^{6}He,2α)2n with four particles in the exit channel one can foresee various reaction channels (e.g. inelastic scattering resulting in ^{6}He excitation and breakup, 1n and 2n transfers, etc.) contributing in the kinematics region where the QFS is detected. In Fig. 1(a) the distribution of momentum value p_{2n} of the center-of-mass (CM) of the two neutrons is shown for the detected events. The p_{2n} momentum is calculated in the anti-lab system, i.e. in the frame moving with the velocity of incoming ^{6}He, p_{2n}^z is the longitudinal component of this momentum along the ^{6}He beam direction and p_{2n}^y is one of its transversal components. Two loci are clearly seen in Fig. 1(a). The first one is located in the QFS region, i.e. close to the zero momentum p_{2n}^z, whereas the second is distributed in the vicinity of $p_{2n}^z \approx -200$ MeV/c. This point approximately corresponds to the CM momentum of the total system α+α+n+n.

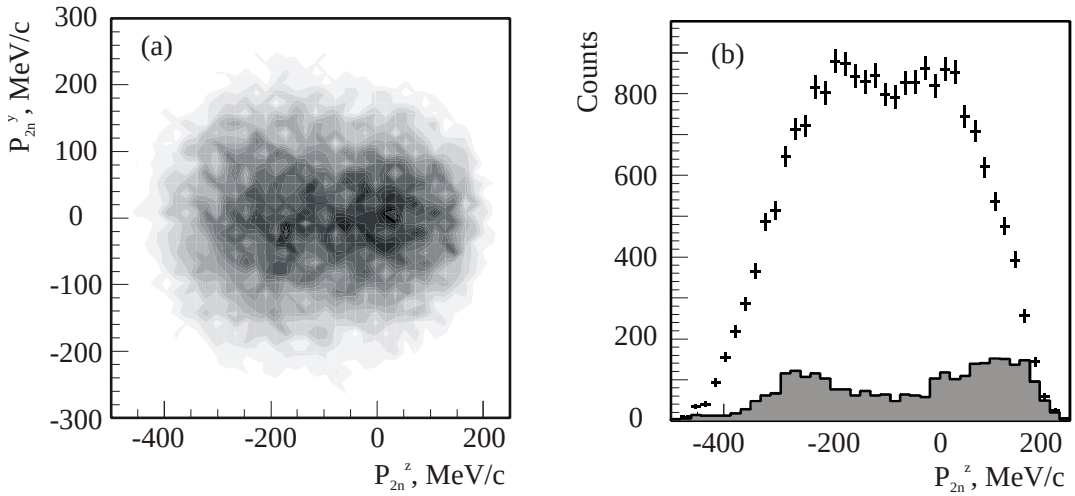

Figure 1.a) the momentum distribution of the two neutron CM p_{2n} obtained for the detected events (see explanations in the text); b) the distribution of longitudinal component of $\vec{p}_{2n}$ obtained for all detected events (points with error bars) and for events selected at a condition $E_{n\text{-}n}$<5 MeV (grey histogram).

In the projection of this distribution onto p_{2n}^z axis made for all detected events (shown in Fig. 1(b) by points with error bars) the two loci heavily overlap. The distribution shown by the grey histogram in the Fig.1(b) is obtained for events with small n-n relative energy $E_{n\text{-}n}$<5 MeV. Two more or less separated peaks are seen in this distribution. The left peak centered at negative p_{2n}^z originates from the 2n-transfer reaction from ^{6}He to ^{4}He with the formation of the first $J^\pi=2^+$ resonance state of ^{6}He. The right pick corresponding to the 2n system with small p_{2n} values can be assigned to QFS.

For the data analysis we performed complete Monte-Carlo (MC) simulation of the reaction studied. In this simulation we used a standard PWIA formalism based on the following T matrix factorization:

$$\frac{d\sigma}{d\Omega_{\alpha-\alpha}}^{QFS} \propto S^2(\vec{p}_{n-n}, \vec{p}_{2n}) \frac{d\sigma}{d\Omega_{\alpha-\alpha}}^{free} F_{PS} dE_{n-n} dE_{\alpha-\alpha} d\Omega_{2\alpha-2n} d\Omega_{n-n}, \qquad \textbf{(1)}$$

where $F_{PS} = \sqrt{E_{n-n} E_{\alpha-\alpha} (E_0 + Q - E_{n-n} - E_{\alpha-\alpha})}$ is the phase space factor taking into account the energy conservation law, $E_0=E_{n\text{-}n}+E_{\alpha\text{-}\alpha}+E_{2\alpha\text{-}2n}-Q$ – the total CM energy of the α+α+n+n system, $S(\vec{p}_{n-n}, \vec{p}_{2n})$ is the spectral function which represents the probability density for the 2n system to be found in a final state characterized with momentum vectors $\vec{p}_{n-n}$ and $\vec{p}_{2n}$. The subscript 2α-2n relates to the motion of the CM of α-α pair in respect to the CM of the two neutrons. The cross section of α-α elastic scattering was calculated for the relative energy $E_{\alpha\text{-}\alpha}$ between two detected α-particles, i.e. the use was made of the post collision prescription.

Due to the large acceptance provided by the detection system the two α particles were observed in wide ranges of their relative energy $E_{\alpha\text{-}\alpha}$ (5 – 60 MeV) and CM scattering angle $\theta_{\alpha\text{-}\alpha}$ (30^o – 150^o). The dependence of the cross-section on $E_{\alpha\text{-}\alpha}$ and $\theta_{\alpha\text{-}\alpha}$ was derived from the known set of phase shifts measured in a proper energy range [10,11,12]. The 2D-matrix $d\sigma/d\Omega_{\alpha\text{-}\alpha} = F(E_{\alpha\text{-}\alpha},\theta_{\alpha\text{-}\alpha})$ used in the simulation is shown in the Fig. 2(a). The angle $\theta_{\alpha\text{-}\alpha}$ was defined as follows:

$$\cos\theta_{\alpha-\alpha} = \frac{\left(\vec{p}_{\alpha-\alpha}^{\,post} \vec{p}_{\alpha-\alpha}^{\,prior}\right)}{\left|\vec{p}_{\alpha-\alpha}^{\,post}\right| \left|\vec{p}_{\alpha-\alpha}^{\,prior}\right|}, \qquad \textbf{(2)}$$

$$\text{where} \quad \vec{p}_{\alpha-\alpha}^{\,prior} = \mu_{\alpha-\alpha}\left(\vec{V}_{6He} + \frac{\left(-\vec{p}_{2n}\right)}{m_\alpha}\right)$$

is the relative momentum between the α particles in the prior collision prescription, $\vec{p}_{\alpha-\alpha}^{\,post}$ is that momentum in the post collision prescription, $\vec{V}_{6He}$ is the lab velocity of ^{6}He and $\mu_{\alpha-\alpha}$ is the reduced mass.

Spectral function containing structure information was calculated taking into account the n-n final state interaction:

$$S(\vec{p}_{n-n}, \vec{p}_{2n}) = \int d\vec{r}_{n-n} d\vec{r}_{2n} \psi^*_{n-n}(\vec{p}_{n-n}, \vec{r}_{n-n}) e^{-i\vec{p}_{2n}\vec{r}_{2n}} \psi_{6He}(\vec{r}_{n-n}, \vec{r}_{2n}), \qquad \textbf{(3)}$$

where $\psi_{6He}(\vec{r}_{n-n}, \vec{r}_{2n})$ is a three-body WF of ^{6}He [8]. Momentum correlations obtained for the spectral function are presented in Fig. 2(b). For comparison in Fig. 2(c) the WF of ^{6}He in the momentum representation is shown. Two intensively populated loci correspond to the di-neutron

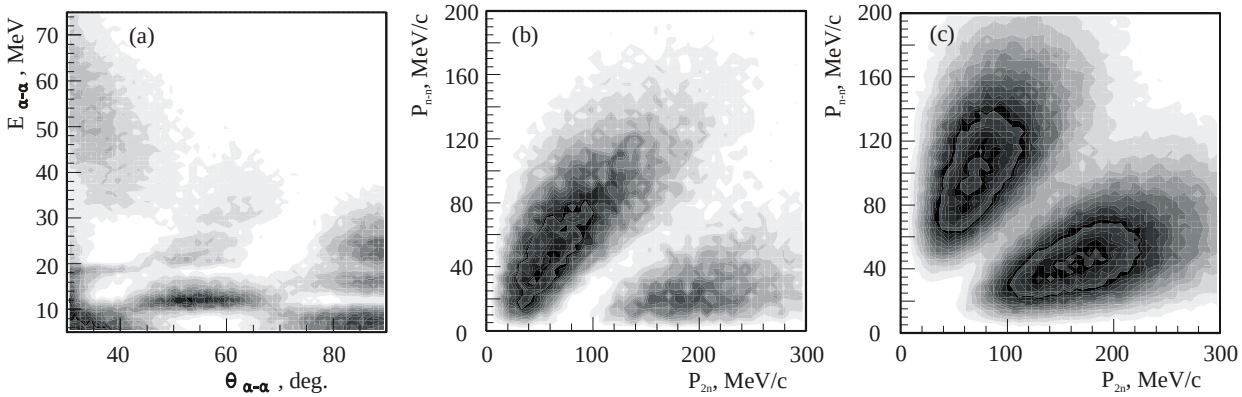

Figure 2. a) $d\sigma/d\Omega_{\alpha\text{-}\alpha}(E_{\alpha\text{-}\alpha},\theta_{\alpha\text{-}\alpha})$ matrix, used in the MC simulation; b) probability of finding two neutrons in states with momentum values p_{n-n} and p_{2n}, obtained from the spectral function (3); c) WF of ^{6}He in the momentum representation.

component of the WF (large p_{n-n}, small p_{2n}) and the cigar-like one (large p_{2n}, small p_{n-n}). The dip between the components arises from the so called Pauli focusing.

Incomplete kinematics conditions were inherent to the present measurements. As a result, only one exit channel, the ^{6}He+^{4}He$\rightarrow^6$He^{2+}+α reaction intervening in the observation of the QFS could be reliably identified. However, though one could not neglect other reaction channels which also contribute in the pattern seen in Fig. 1(a) we will show that this contribution was considerably suppressed by the event selection made with the choice of large α-2n relative energy: $E_{\alpha 1\text{-}2n}$>10 MeV and $E_{\alpha 2\text{-}2n}$>10 MeV. At this choice, the contribution of reaction channels resulting in the population of high-lying continuum excited states in ^{6}He was well described by phase space (PS) of the four-body break-up ^{6}He+^{4}He→α+α+n+n. This selection was used in the presentation made below.

In order to enhance the reliability of data explanation, a set of experimental distributions was simultaneously fitted with the use of MC simulation. This set includes the distributions over eight essentially independent observables relating to the reaction mechanism and the structure of ^{6}He. These are: the total momentum of the 2n CM system p_{2n} and the two projections p^z_{2n} and p^x_{2n}, the relative energies $E_{\alpha\text{-}\alpha}$ and $E_{n\text{-}n}$, the $\theta_{\alpha\text{-}\alpha}$ angle, the Treiman-Yang angle $\theta_{T\text{-}Y}$ [13], and the hyper angle θ_h characterizing in Jacoby coordinates the three-body correlations occurring in ^{6}He: $tg\theta_h = \sqrt{E_{n-n}/\tilde{E}_{2n-\alpha}}$, where $\tilde{E}_{2n-\alpha} = \frac{p^2_{2n}}{2\mu_{2n-\alpha}}$.

Results

Fits were made in the whole ranges of the $E_{\alpha\text{-}\alpha}$ and $E_{n\text{-}n}$ variables. Fig. 3 shows the fit results obtained in the energy ranges 35<$E_{\alpha\text{-}\alpha}$<40 MeV and $E_{n\text{-}n}$<10 MeV. The results of the MC simulations made for the QFS and the four-body PS are shown by dashed and dotted histograms, respectively. The solid histogram is the sum of the QFS and the PS contributions, the points with

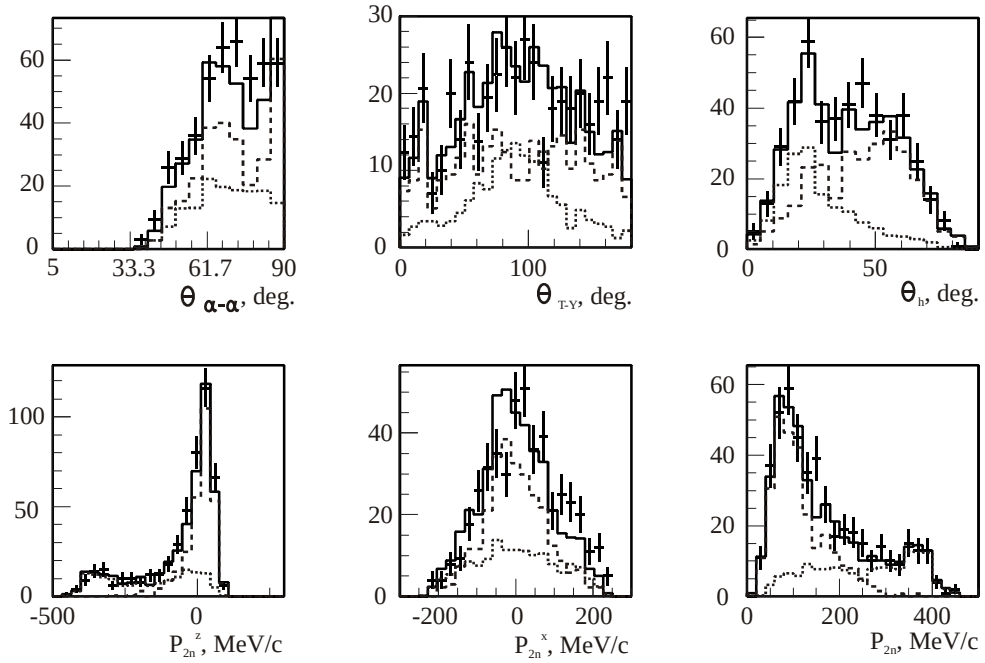

Figure 3. The results of a fit to experimental data obtained in the energy ranges 35< $E_{\alpha\text{-}\alpha}$<40 MeV and $E_{n\text{-}n}$<10 MeV. The QFS contribution is shown by dashed histogram, dotted histogram corresponds to the 4-body PS. Solid histogram is the sum of the QFS and PS contributions, points with error bars show the experimental data.

error bars are the experimental data. One sees that the distributions given by the model are in excellent agreement with the experimental data.

A good agreement was also obtained in the fits performed in other ranges of $E_{\alpha\text{-}\alpha}$ and $E_{n\text{-}n}$. The ratio of the experimental cross-section $d\sigma/d\Omega_{\alpha\text{-}\alpha}$ extracted from the data with the use of the eq. (1) to that of the free α-α elastic scattering was found to be constant within a factor of 30% in the whole energy range $10<E_{\alpha\text{-}\alpha}<50$ MeV and $0<E_{n\text{-}n}<40$ MeV.

A good test for the applicability of Eq. (1) makes the comparison of the angular dependence calculated for the free α-α elastic scattering cross section with the dependence measured in the experiment. In Fig. 4 shown are angular distributions obtained in various $E_{\alpha\text{-}\alpha}$ ranges with a condition of $E_{n\text{-}n}<10$ MeV imposed. Angular distribution characterizing the QFS is sensitive to the $E_{\alpha\text{-}\alpha}$ value and has specific shapes, strongly varying within the $E_{\alpha\text{-}\alpha}$ energy range measured in the experiment. At the same time, the α-α elastic scattering cross sections vary by more than 2 orders of magnitude within the energy and angular ranges covered by the acceptance of the detection system used in these measurements. It is seen in Fig. 4 that the MC simulation well reproduces the essential features of the experimental distributions.

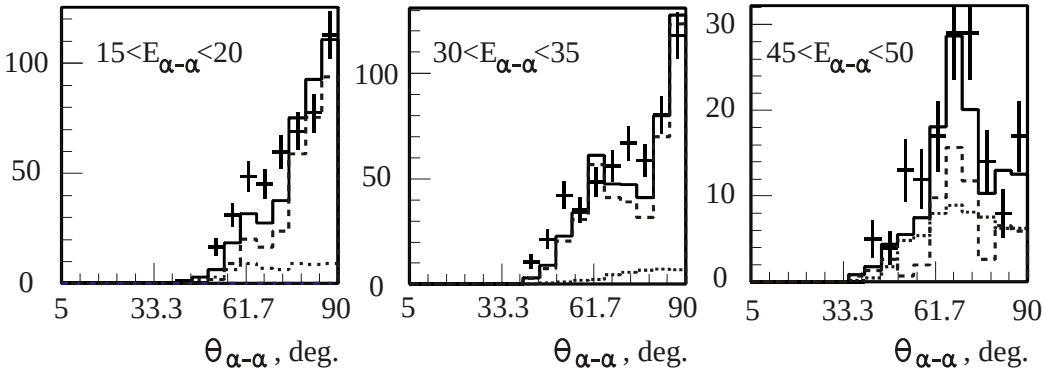

Figure 4. The angular dependences of the cross-section of the QFS measured at different energies $E_{\alpha\text{-}\alpha}$ for the n-n relative energy $E_{n\text{-}n}<10$. The QFS contribution is shown by the dashed histogram, the dotted one corresponds to the 4-body PS. The solid histogram is the sum of the QFS and the PS contributions, the points with error bars are the experimental data.

In order to check if the angular distributions presented in Fig. 4 are sensitive to the choice of axis from which the $\theta_{\alpha\text{-}\alpha}$ angle is reckoned, we compare in Fig. 5 the experimental $\theta_{\alpha\text{-}\alpha}$ distributions presented in Fig. 4 (points with error bars) with similar distributions emerging from

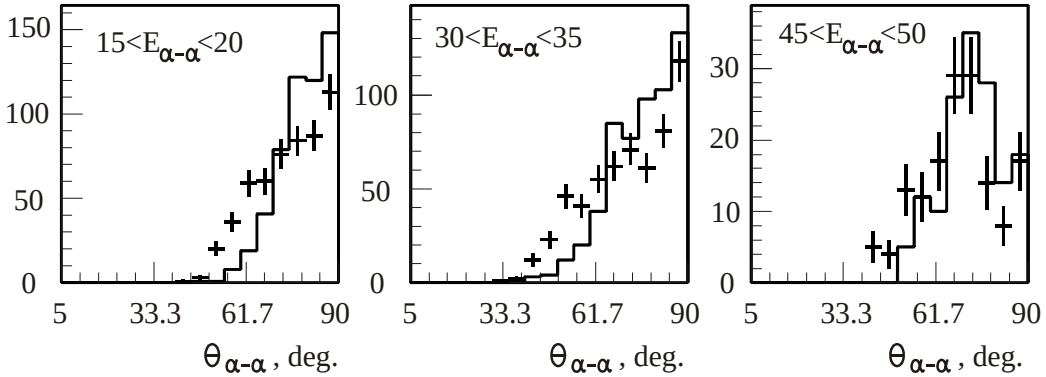

Figure 5. Experimental angular dependence of the QFS cross section obtained for different $E_{\alpha\text{-}\alpha}$ bins at fixed n-n relative energy $E_{n\text{-}n}<10$. Points with error bars show the experimental distribution obtained by taking angle $\theta_{\alpha\text{-}\alpha}$ defined in Eq. (2). The case with angle $\theta_{\alpha\text{-}\alpha}$ calculated from Eq. (4) is shown by solid histogram.

MC simulation made with angle $\theta_{\alpha\text{-}\alpha}$ defined in respect to the direction of the momentum vector of ^{6}He $\vec{p}_{6He}$ taken in lab system:

$$\cos\theta_{\alpha-\alpha} = \frac{\left(\vec{p}^{\,post}_{\alpha-\alpha}\vec{p}_{6He}\right)}{\left|\vec{p}^{\,post}_{\alpha-\alpha}\right|\left|\vec{p}_{6He}\right|}. \qquad \textbf{(4)}$$

The latter distributions are shown in Fig. 5 by solid histograms. At large α-α relative energy $45<E_{\alpha\text{-}\alpha}<50$ MeV the angles $\theta_{\alpha\text{-}\alpha}$ defined according to eqs. (2) and (4) are very close one to another and the two angular distributions practically coincide. At lower $E_{\alpha\text{-}\alpha}$ the dependences of the cross-section on the angle reckoned from the direction of the momentum $\vec{p}_{6He}$ have no any noticeable features in comparison with those on the angle defined in respect to the direction of the momentum $\vec{p}^{\,prior}_{\alpha-\alpha}$. One should note that at E_0~60 MeV the vector $\vec{p}^{\,prior}_{\alpha-\alpha}$ strongly depends on the internal motion of α-particle bound in ^{6}He and varies for each individual event whereas the vector $\vec{p}_{6He}$ is fixed. More pronounced structure of the distribution for the angle $\theta_{\alpha\text{-}\alpha}$ can be considered as the evidence in favor of the assumption that just the vector of the momentum $\vec{p}^{\,prior}_{\alpha-\alpha}$ defines a real direction of the collision in the input reaction channel.

In Fig. 6 we present the results of fits to the experimental distributions in momentum p_{2n} and hyper angle θ_h obtained at a condition of the full $E_{n\text{-}n}$ range and $30<E_{\alpha\text{-}\alpha}<35$ MeV. The fits were made with the use of two different MC simulations. In Figs. 6(c) and (d) dashed histograms show the contribution of the QFS obtained with the use of spectral function (3); dotted histograms correspond to the four-body PS. The assumed contribution of the T=2 excited state of ^{8}Be, which could be populated in the 2p transfer from ^{4}He to ^{6}He, is shown by the dash-dotted histogram. The fit presented in Figs. 6 (a) and (b) was made with the use of Eq. (1) and spectral function replaced by the WF of ^{6}He in the momentum representation (see Fig. 2(c)). One sees that this fit is considerably less consistent with the experimental data. Particularly, the dip between the di-neutron and cigar-like components visible in the simulated θ_h distribution was not observed in the experiment.

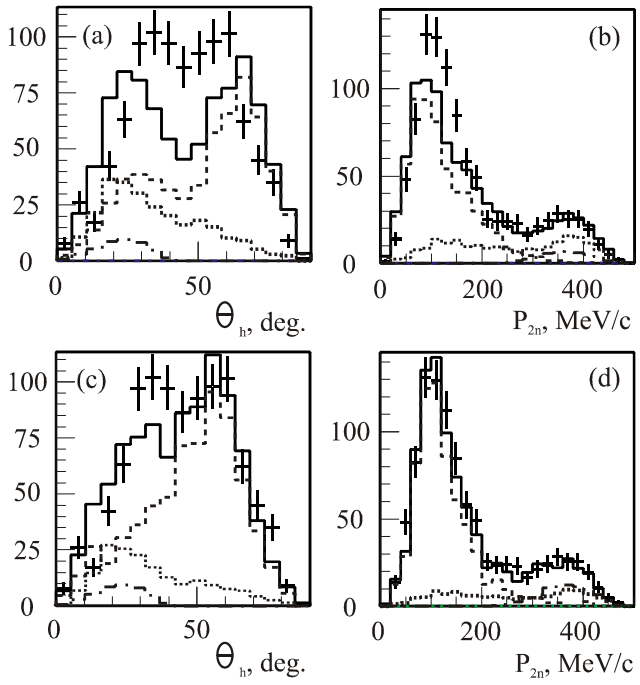

Figure 6. The hyper angle θ_h and momentum p_{2n} distributions obtained in energy range $30< E_{\alpha\text{-}\alpha}<35$ MeV. The QFS contribution presented by dashed histograms was obtained with the use of spectral function (3) (panels (c) and (d)) and with the use of the ^{6}He WF (panels (a) and (b)).

Summary

In our experiment the QFS of the α core bound in ^{6}He was explored keeping in mind the possible study of the structure of this neutron drip nucleus. Possible use of QFS for revealing momentum correlations specific for three-body Borromean nuclei was the subject of our interest. The three-body WF of ^{6}He is believed to be well established in theory and a comparison of theoretical predictions with experimental data could be a good test for the convenience of QFS for the study of cluster states of halo nuclei.

For the first time coincident α particles arising in the ^{4}He(^{6}He,2α)nn reaction were detected in a wide angular range providing for a wide kinematical range of the measured angular and momentum distributions. The contribution of reactions competing with QFS in the α+α+n+n output channel was considerably suppressed by the selection of events with large α-2n relative energy $E_{\alpha\text{-}2n}$>10 MeV. This condition provided for the reliable separation of events corresponding to the QFS reaction. The experimental distributions of a number of observables relevant to the reaction mechanism and the structure of ^{6}He were compared with the results of the MC simulation based on the PWIA formalism. It was established that PWIA predictions are well consistent with experimental data when the n-n FSI is taken into account. Due to the n-n FSI such a pronounced peculiarity of the ^{6}He WF as Pauli focusing is not observed.

The ratio of the experimental cross-section $d\sigma/d\Omega_{\alpha\text{-}\alpha}$ to that of the free α-α elastic scattering was found to be constant in energy ranges $10<E_{\alpha\text{-}\alpha}<50$ MeV and $0<E_{n\text{-}n}<40$ MeV. The angular distributions of quasifree α-α scattering measured for different energies $E_{\alpha\text{-}\alpha}$ are well reproduced by the MC simulation while the relative value of the α-α elastic scattering cross-section varied by more than 2 orders of magnitude within the energy and angular ranges corresponding to the acceptance of the detection system.

Acknowledgement

This work was partly supported by the Russian Foundation for Basic Research Grant No. 05-02-16404 and by the INTAS Grant No. 03-51-4496.

References

1. P.G. Roos, N.S. Chant, A.A. Cowley et al., Phys. Rev. **C15** (1977) 69.
2. C.W. Wang, N.S. Chant, P.G. Roos et al., Phys.Rev. **C21** (1980) 1705.
3. G. Jacob and Th.J. Maris, Rev. of Mod. Phys. **38** (1966) 121.
4. N.S. Chant and P.G. Roos, Phys. Rev. **C15** (1977) 57.
5. A. Okihana, K. Ushiro, T. Yoshimura et al., Nucl. Phys. **A614** (1997) 71.
6. M.V. Zhukov, B.V. Danilin, D.V. Fedorov et al., Phys. Rep. **231** (1993) 151.
7. R.E. Warner, A. Okihana, M. Fujiwara et al., Nucl. Phys. **A503** (1989) 161.
8. R.E. Warner, E. Cheung, C.F. Perdrisat et al., Phys. Rev. **C42** (1990) 2143.
9. A.M. Rodin et al., Nucl. Instr. Meth. **A391** (1997) 228.
10. T.A. Tombrello and L.S. Senhouse, Phys. Rev. **129** (1963) 2252.
11. A.D. Bacher, F.G. Resmini, H.E. Conzett et al., Phys. Rev. Lett. **29** (1972) 1331.
12. P. Darriulat, G. Igo, H.G. Pugh and H.D. Holmgren, Phys. Rev. **137**, (1965) 315.
13. R.B. Liebert, K.H. Purser and R.L. Burman, Nucl. Phys. **A216** (1973) 335.